This is a repository copy of *Carbon Nitride as a Ligand: Selective Hydrogenation of Terminal Alkenes using [(η5-C5Me5)IrCl(g-C3N4-κ2N, N')]Cl:Selective Hydrogenation of Terminal Alkenes using [(η5-C5Me5)IrCl(g-C3N4-κ2N, N')]Cl*.

White Rose Research Online URL for this paper:
https://eprints.whiterose.ac.uk/id/eprint/157200/

Version: Accepted Version

FULL PAPER

Carbon Nitride as a Ligand: Selective Hydrogenation of Terminal Alkenes using [(η^5-C$_5$Me$_5$)IrCl(g-C$_3$N$_4$–κ^2 *N, N'*)]Cl

Ben Coulson,[a] Leonardo Lari,[b] Mark Isaacs,[c] Daniel J. Raines,[a] Richard E. Douthwaite*[a] and Anne-K. Duhme-Klair *[a]

[a] Dr. B. Coulson, Dr. D.J. Raines, Dr. R.E.Douthwaite, Prof. A.-K., Duhme-Klair
     Department of Chemistry
     University of York
     York, YO10 5DD, UK
     E-mail: richard.douthwaite@york.ac.uk
[b] Dr. L. Lari
     Department of Physics
     University of York
     York, YO10 5DD, UK
[c] Dr. M. Isaacs
     HarwellXPS, R92 Research Complex at Harwell
     Rutherford Appleton Laboratories
     Harwell, Didcot, OX11 0QS, UK, and
     Department of Chemistry
     University College London
     20 Gordon Street, London, WC1H 0AJ, UK

     Supporting information for this article is given via a link at the end of the document.

Abstract: Anchoring a homogeneous catalyst onto a heterogeneous support facilitates separation of the product from the catalyst, and catalyst-substrate interactions can also modify reactivity. Herein we describe the synthesis of composite materials comprising carbon nitride (g-C$_3$N$_4$) as the heterogeneous support and the well established homogeneous catalyst moiety [Cp*IrCl]$^+$ (where Cp* = η^5-C$_5$Me$_5$), commonly used for catalytic hydrogenation. Coordination of [Cp*IrCl]$^+$ to g-C$_3$N$_4$ occurs directly at exposed edge sites with a κ^2 *N, N'* binding motif, leading to a primary inner coordination sphere analogous to known homogeneous complexes of the general class [Cp*IrCl(NN–κ^2 *N, N'*)]$^+$ (where *N, N'* = a bidentate nitrogen ligand). Hydrogenation of unsaturated substrates using the composite catalyst is selective for terminal alkenes, which is attributed to the restricted steric environment of the outer coordination sphere at the edge-sites of g-C$_3$N$_4$.

Introduction

Graphitic carbon nitrides (g-C$_3$N$_4$s) are two-dimensional compounds that are readily produced from a range of abundant nitrogen-containing organic precursors. These materials are attracting increasing attention due to their potential applications in catalysis, water purification, biosensing and imaging.[1]

Many applications of g-C$_3$N$_4$ require metal funtionalization, which can be achieved via adsorption or linking covalently to defect functionalities or intraplanar binding sites. (Figure 1). For catalytic applications, C$_3$N$_4$ has been functionalized with metal atoms, nanoparticles, and metal complexes, either adsorbed or anchored onto g-C$_3$N$_4$ using an organic linking group (Figure 1a-c). For example, single metal atom catalysts of cobalt, palladium, ruthenium and iridium can be bound at intraplanar sites defined by adjoining heptazine units (Figure 1a),[2] and applied to electrocatalytic reduction and the hydrogenation of alkynes.[3] Iron, and copper analogues have also been applied to Fenton-like
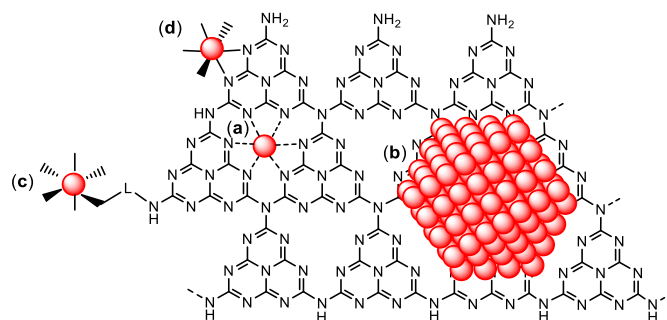
oxidation chemistry.[4] Metal nanoparticles are active cocatalysts when adsorbed onto g-C$_3$N$_4$ (Figure 1b) for photocatalytic hydrogen production.[5] Metal complex catalysts have also been anchored to g-C$_3$N$_4$ *via* ancillary ligands (Figure 1c) and applied to photocatalytic proton and carbon dioxide reduction.[6]

More recently, we have demonstrated the selective functionalization of g-C$_3$N$_4$ *via* direct coordination of a metal complex fragment (Figure 1d).[7] Reaction between [Re(CO)$_5$Cl] and g-C$_3$N$_4$ gave [ReCl(CO)$_3$(g-C$_3$N$_4$-κ^2 *N, N'*)], where *N, N'*-bidentate coordination of Re was assigned based on the IR spectroscopic characteristics of the carbonyl ligands. It was found that due to the relative size of [ReCl(CO)$_3$] (*ca.*5.5 Å) compared to the interplanar distance of adjacent g-C$_3$N$_4$ layers (3.25 Å), steric constraints limit coordination to the exposed *N, N'* edge sites of heptazine moieties.

Figure 1. Functionalization of g-C$_3$N$_4$ with a) a single atom, b) a metal nanoparticle, c) a metal complex with covalent linker (L), and d) direct coordination.

Consequently, we have been motivated to exploit the *N, N'* binding motif and steric constraints imposed by the g-C$_3$N$_4$ microstructure for catalysis, essentially using g-C$_3$N$_4$ directly as

an ancillary chelating ligand. Chelating *N, N'* bidentate ligands are used to support a range of homogenous catalytic reactions including molecular complexes of the class [Cp*IrCl(NN-κ^2 *N, N'*)], which have been used extensively as precatalysts for transfer hydrogenation,[8] and to a much lesser extent direct hydrogenation of aldehydes, ketones[9] and carbon dioxide.[10] The *N, N'* ligand can sterically modify metal-substrate interactions to control regio-, chemo- and stereoselective hydrogenation.

Herein, we describe the direct coordination of [Cp*IrCl]$^+$ (where Cp* = η^5-C$_5$Me$_5$) to g-C$_3$N$_4$ and the application of the resulting materials to the catalytic hydrogenation of unsaturated molecules and show that direct coordination of [Cp*IrCl]$^+$ to g-C$_3$N$_4$ produces a material that catalyses the selective hydrogenation of terminal alkenes.

Results and Discussion

Synthesis and Characterization: Typically, complexes of the class [Cp*IrCl(*NN*-κ^2 *N, N'*)]$^+$ are prepared by reaction between the respective *N, N'* ligand and the iridium-containing precursor [Cp*IrCl$_2$]$_2$, often followed by chloride exchange to give [Cp*IrCl(*NN*-κ^2 *N, N'*)]X (where X = PF$_6^-$, BF$_4^-$, etc).[8d] Chloride exchange supports catalysis by increasing the solubility of the resulting complex and electrophilicity for substrate binding.

Reaction between g-C$_3$N$_4$ and [Cp*IrCl$_2$]$_2$ in ethanol under reflux gave the Ir complex-decorated carbon nitride (**1**), with characterization data consistent with the formulation [Cp*IrCl(g-C$_3$N$_4$-κ^2 *N, N'*)]Cl (*vide infra*) (Scheme 1). To prepare a derivative resulting from anion exchange, reaction between [Cp*IrCl$_2$]$_2$ and AgPF$_6$ forms the putative [Cp*IrCl][PF$_6$], which was then added to g-C$_3$N$_4$ to give [Cp*IrCl(g-C$_3$N$_4$-κ^2 *N, N'*)][PF$_6$] (**2**) (Scheme 1).
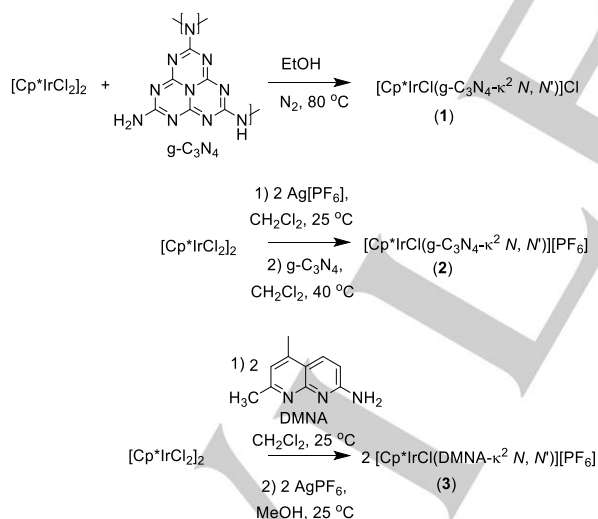

Scheme 1. Synthesis of materials **1** and **2**, and complex **3**.

The iridium complex loading for **1** and **2** was determined using a combination of ICP-MS (iridium) and ion exchange chromatography (chlorine and fluorine). ICP-MS analysis gave almost identical iridium loadings of 1.34 and 1.33 wt% for **1** and **2**, respectively. The synthesis of both **1** and **2** was undertaken using an excess of [Cp*IrCl$_2$]$_2$, which indicates that complexation occurs selectively at the same binding sites for both iridium precursors.

The chlorine loading of 0.37 and 0.21 wt% for **1** and **2**, respectively and fluorine loading of 1.9 wt% for **2**, are equivalent to Ir:Cl and Ir:Cl:F ratios of 1:1.9 and 1:1.1:5.3 for **1** and **2**, respectively, consistent with the proposed formulations.

To probe the surface speciation, XPS data of **1** and **2** were compared with data obtained for g-C$_3$N$_4$. Very similar nitrogen 1s spectra (Figure S1a, Supporting Information) showed components at binding energies of 398.7, 400.0, and 401.2 eV, which are attributable to CNC, CN$_3$ and CNH, respectively, consistent with reported data for g-C$_3$N$_4$.[11] The carbon 1s spectra (Figure S1b, Supporting Information) also show signals at 284.6, and 288.4 eV attributable to carbonaceous (graphitic) impurity and CNC of g-C$_3$N$_4$, respectively. An additional peak at 285.9 eV for **1** and **2**, attributable to C-C and C-H bonds, are consistent with the presence of a Cp* moiety. More clearly, the iridium 4f spectra (Figure 2) of **1** and **2** both give two peaks arising from spin orbit coupling at binding energies (BE) of 62.5 and 65.4 eV. Reported BE for [Cp*Ir(bipy)Cl]Cl}[12] and related triazine-bipyridine}[12] and phenanthroline frameworks [13], coordinating [Cp*IrCl]$^+$ moieties all give BE of 62.1 and 65.1 eV compared to BE of 62.3 and 65.2 eV for the more directly relevant a heptazine framework analogue.[14] These data indicate less electron density is donated by the heptazine and related g-C$_3$N$_4$ ligand in comparison to other common κ^2 *N,N* donor ligands and support the hypothesis that κ^2 *N,N* binding to edge sites of g-C$_3$N$_4$ is relatively weak.[7] The BE of the precursor [Cp*IrCl]$_2$ (61.8 and 64.8 eV, Figure S1c) are clearly distinct from **1** and **2** showing that reaction between [Cp*IrCl]$_2$ and g-C$_3$N$_4$ has occurred and not simply adsorption. Furthermore, the full width half maximum of each peak is consistent with a monometallic moiety and, notably, there is no evidence of iridium oxide or metal particle formation.
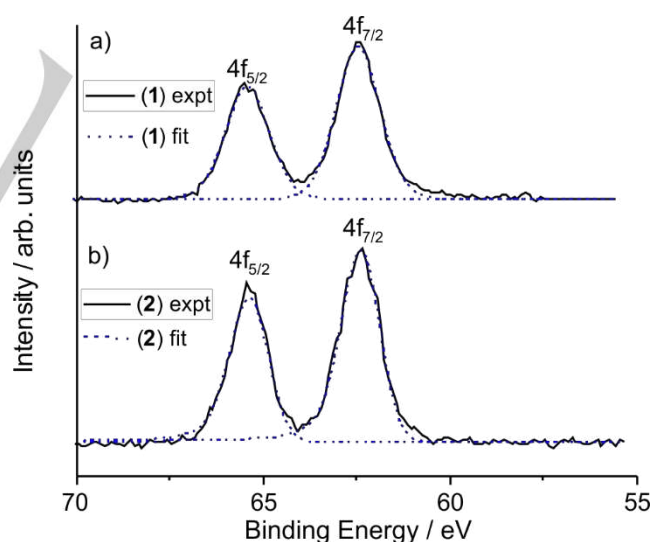
Figure 2. XPS spectra (iridium 4f region) of a) **1** and b) **2**

^{13}C CP-MASNMR spectra of **1**, **2** and g-C$_3$N$_4$ show signals at δ 156.7 and 164.6 ppm, attributable to N$_2$CNH$_x$ and CN$_3$ environments, respectively, previously reported for g-C$_3$N$_4$.[15] For **1** and **2**, additional signals are observed at δ 12.0 and 88.2, and 9.4 and 89.3 ppm, consistent with Cp* CH$_3$ and ring C-atoms, respectively (Figure 3), and compare to δ 11.1 and 87.1 ppm found for [Cp*IrCl$_2$]$_2$ (Figure S2a, Supporting Information). The chemical shifts of the ring C-atom signals are sensitive to the

metal and oxidation state and the comparable data of **1**, **2** and [Cp*IrCl₂]₂ strongly suggest all coordinate to an iridium(III) ion.

Determination and comparison of zeta potentials at pH 7 in water was used to indirectly study the surface charge of g-C₃N₄, **1** and **2**. There is a clear difference between the potential of g-C₃N₄ (-28.7 ± 0.8 mV), and the Ir complex decorated materials **1** (27.7 ± 0.8 mV) and **2** (32.5 ± 0.3 mV). The negati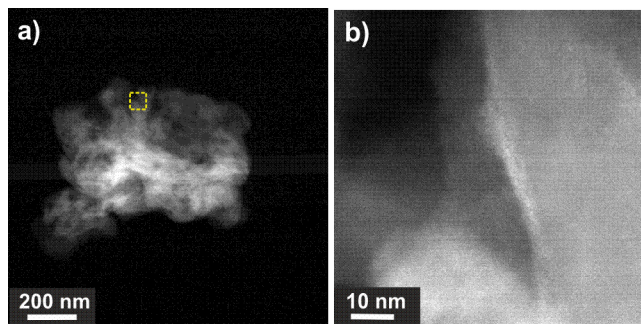ve potential of g-C₃N₄ is very similar to that reported at pH 7 for various other carbon nitrides and has been attributed to negative charges at edge sites of incompletely condensed g-C₃N₄ arising from water dissociation equilibria.[16] Addition of [Cp*Ir(III)Cl]⁺ complex moieties causes a significant positive shift in potential, consistent with addition of a positively charged species to edge sites. The similar values of **1** and **2** again indicate very similar formulations suggesting that for **1** a chloride ion has dissociated and coordination of g-C₃N₄ exhibits the κ² *N, N'* binding mode.

Figure 4. a) HAADF images of **1**; b) higher magnification of the area within the yellow box in image a).

Figure 3. ¹³C CP-MASNMR spectra of a) **1**; b) **2**; and c) g-C₃N₄. * Indicates spinning side-bands.

Furthermore, powder X-ray diffraction (PXRD) data and scanning electron microscopy (SEM) images of g-C₃N₄, **1** and **2** (Figures S3 and S4, Supporting Information) are indistinguishable indicating intercalation has not occurred. Collectively, the data confirm that metal complex functionalization occurs on the surface of g-C₃N₄ and are consistent with similarly charged formulations [Cp*IrCl(g-C₃N₄ -κ² *N, N'*)]Cl (**1**) and [Cp*IrCl(g-C₃N₄-κ² *N, N'*)][PF₆] (**2**).

The distribution of [Cp*IrCl]⁺ across the surface of g-C₃N₄, was studied using scanning transmission electron microscopy (STEM) coupled with Energy Dispersive X-ray (EDX) to image and identify the distribution of iridium and chlorine in **1**. High Angle Annular Dark Field (HAADF) imaging (Figure 4) and EDX (Figure S5, Supporting Information) show that iridium and chlorine atoms are found in the same regions of **1** and are concentrated at the edges of g-C₃N₄ particles.

The binding mode of g-C₃N₄ to a [Cp*IrCl]⁺ moiety, was modelled using a complex of the commercially available ligand 5, 7-dimethyl-[1, 8]-naphthyridine-1-amine (DMNA) (Scheme 2). DMNA exhibits various metal-binding modes, including monodentate, bidentate and tridentate via a combination of heterocyclic nitrogen and amino functionalities.[17] Analogous binding modes are conceivable for g-C₃N₄, and comparison of ¹³C CP-MAS NMR data could provide additional insight into the binding of g-C₃N₄ in **1** and **2**.

Reaction between DMNA and [Cp*IrCl₂]₂ gave [IrCp*Cl(DMNA–κ² *N, N'*)][PF₆] (**3**) (Scheme 2). A single crystal structure determination (Figure 5, and Tables S1-8, Supporting Information) confirmed the proposed formulation. The geometry at the iridium atom is a *pseudo*-octahedral piano stool, analogous to related [Cp*IrCl(NN)] complexes of bidentate κ² *N, N'* ligands, such as 8-naphthyridine (napy) [Cp*IrCl(napy)][PF₆][18] and 2, 2'-bipyridine (bpy) [Cp*IrCl(bpy)][ClO₄].[19] Of direct relevance, the ¹³C CP-MAS NMR spectrum of **3** (Figure S2b, Supporting Information) shows resonances at δ 9.9 and 89.3 ppm, which are very similar to those of **1** and **2**, corroborating formulation of bidentate coordination of g-C₃N₄ to [Cp*IrCl]⁺. Furthermore Ir 4f XPS of **3** gave BE of 62.3 and 65.3 eV (Figure S1d) very similar to **1** and **2** supporting the hypothesis that [Cp*IrCl]⁺exhibits κ²-N, N' binding to g-C₃N₄.
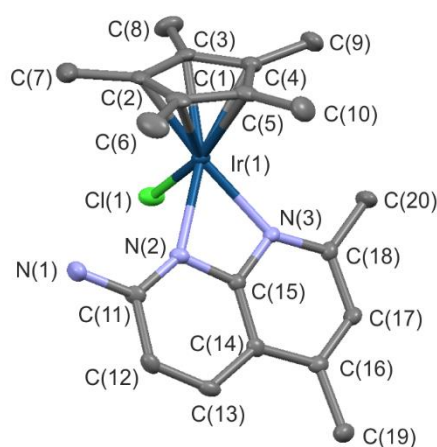
Figure 5. Molecular structure of [IrCp*Cl(DMNA-κ² *N, N'*)][PF₆] (**3**). Thermal ellipsoids are at 50 % probability level and hydrogen atoms are omitted for clarity.

Catalysis: Soluble metal complexes that incorporate [Cp*Ir(*NN*)] moieties have been investigated extensively as homogeneous precatalysts for hydrogenation reactions, particularly transfer hydrogenation of polar unsaturated bonds.[8-10] In addition, [Cp*IrCl]+ has been incorporatedas a cofactor in artificial metalloenzymes, exploiting the chiral enzyme environment for enantioselective transfer hydrogenation of imines.[20] Furthermore, [Cp*IrCl]+ has also been coordinated to frameworks based on covalent triazine, heptazine and phenanthroline and applied to transfer hydrogenation of ketones[21] and direct hydrogenation of carbon dioxide to formate.[13, 22] We were motivated to explore g-C₃N₄ for hydrogen-related catalysis because of the demonstrated photocatalytic proton/hydrogen reactivity of g-C₃N₄ that may potentially support thermal hydrogenation chemistry. Thermal catalytic hydrogenation using metal-g-C₃N₄ systems are still rather limited in number but there are clear opportunities, as demonstrated by metal nanoparticle (M_{NP}) and single metal atom catalysis (M_{SAC}) supported on g-C₃N₄.[2, 23] Examples include M_{NP} of Pd,[24] Pt,[25] Pd₃S,[26] NiW₂C,[27] for substrates including nitriles, [24a] phenylacetylene,[24b] acetylene,[26] 1,5-cyclooctadiene.[24c] phenols,[24d, 24e] nitriarenes,[27] quinolone,[24g] dioxygen,[24f] and CO₂.[24h, 24i] M_{SAC} of Pd$_{SAC}$,[3b, 28] Ir$_{SAC}$,[29] and Ru$_{SAC}$,[30] catalyse dihydrogen reduction of alkynes, [3b, 28] nitroarenes[3b] furfaral,[29] and vanillin[30]

For all hydrogenation and transfer hydrogenation reactions in this study, unmodified g-C₃N₄ did not show any catalytic activity under the conditions tested; only complexes and materials containing iridium gave detectable quantities of product. Initially, transfer hydrogenation in water was explored using an established reaction between [NH₄]CO₂H as the hydrogen source and the water soluble substrate methyl-6, 7-dimethoxy-3, 4-dihydroisoquinoline. However, even though **1** and **2** catalyse transfer hydrogenation (Figure S6, Supporting Information), recycling studies showed significant leaching of the iridium complex fragment in water. Therefore, the stability of **1** and **2** was investigated in a range of solvents (Figure S7, Supporting Information), which revealed that the use of non-polar solvents does not result in detectable leaching. Hence, subsequent hydrogenation reactions were performed in hexane.

Initially, using **1 – 3** and [Cp*IrCl₂]₂, the hydrogenation of three alkenes, styrene, α-methyl styrene, and trans-β-methyl styrene (Table 1), was carried out at 25 ºC and 10 bar H₂ for 1 hour to initially differentiate catalyst and substrate activity using non-optimized conditions. Gas chromatographic analysis revealed that **3** and [Cp*IrCl₂]₂ gave only traces of product, presumably because as insoluble microcrystalline solids most of the iridium is inaccessible to the substrate. However, **1** and **2** catalyse hydrogenation of the terminal alkenes styrene and α-methyl styrene, with **1** more active than **2**, whereas neither catalyse hydrogenation of trans-β-methyl styrene. The hydrogenation of styrene is slow, occurring with turn over frequencies (TOF) of 50 and 20 hr⁻¹, respectively.

The substrate scope investigation with **1** showed that only terminal alkenes are hydrogenated. Hydrogenation of other substrates, such as acetophenone, benzaldehyde, benzonitrile, phenylacetylene, and 1-octyne did not occur under the test conditions. Other internal alkenes, such as cyclohexene and 2-octene were also unaffected, as was the diene 3-methyl-1, 3-pentadiene, whereas 1-octene was hydrogenated, but more slowly than styrene with TOF = 25 h⁻¹. Addition of one equivalent

Table 1. Comparison of the catalytic activity of [IrCp*Cl₂]₂, **1 – 3** for the hydrogenation of selected styrenes.[a]

Catalyst	Substrate	Con[b] (%)	TOF (hr⁻¹)
[Cp*IrCl₂]₂	Styrene	5[a]	5[a]
1	Styrene	50	50
2	Styrene	20	20
3	Styrene	0	0
[Cp*IrCl₂]₂	α-methyl styrene	7	7
1	α-methyl styrene	37	37
2	α-methyl styrene	44	44
3	α-methyl styrene	0	0
[Cp*IrCl₂]₂	β-methyl styrene	6	6
1	β-methyl styrene	6	6
2	β-methyl styrene	5	5
3	β-methyl styrene	0	0

[a]Conditions: catalyst (2 μmol of iridium), substrate (0.2 mmol), hexane (1 mL), H₂ (10 bar), 25 ºC. Determined by GC; [b]conversion after 1h

of benzaldehyde and acetophenone reduces the TOF of styrene hydrogenation to 3 and 15 h⁻¹, respectively, and addition of phenyl acetylene and 1-octyne, prevents styrene hydrogenation. These competition reactions suggest that carbonyl-containing substrates reversibly compete for coordination sites at the iridium atom, whereas alkynes bind or react essentially irreversibly. Of note, for the internal alkenes, no alkane or alkene products arising from isomerizsation are observed.

The selectivity of **1** is exemplified by hydrogenation of (R)-(+)-limonene (Fig 6) a valuable chemical feedstock,[31] that gives exclusively (R)-(+)-p-meth-1-ene with >99% yield. Selective partial hydrogenation of limonene has been extensively investigated and is very sensitive to reaction conditions, often resulting in additional reduction or isomerizsation. The most selective systems reported are metal nanoparticle heterogeneous catalysts supported on carbon substrates, such as palladium, ruthenium and platinum, which give up to 83% selectivity for the reduction of (R)-(+)-limonene to (R)-(+)-p-meth-1-ene, which is increased to 95% for platinum on SiO₂ at conversions > 95%.[32] Nickel, ruthenium, and platinum on graphene in supercritical CO₂ give selectivity up to 91%, but at conversions < 50%.[33] For rhodium nanoparticles on montmorillonite clay, conversion and selectivity (>99%) can be obtained with careful control of hydrogen pressure and TOF = 273 hr⁻¹.[34] Ionic liquid coated ruthenium nanoparticles on Al₂O₃ give >99% conversion and selectivity with very high catalyst loading.[35] Therefore, hydrogenation of limonene with **1** is amongst the most selective and it is achieved with low (1.34 wt%) iridium loading.

To investigate the reaction in more detail, styrene was hydrogenated using **1** and a 1:1 mixture of D₂:H₂. According to ²H NMR and GC-MS data (Figures S8 and S9, Supporting Information), mono-deuterated ethylbenzene was obtained, showing that the hydrogenation mechanism is not concerted, since H-H bond cleavage is separate to hydrogen transfer to
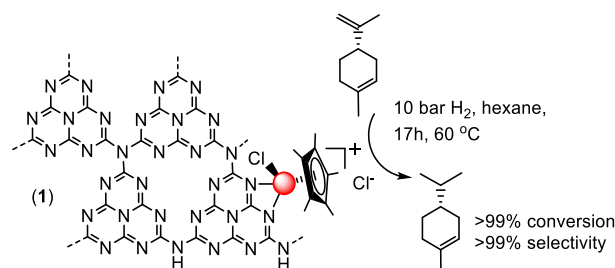
Figure 6. Proposed edge-site coordination of [Cp*IrCl]+ to g-C$_3$N$_4$ and selective hydrogenation of limonene.

styrene. Further work will be required to elucidate the origin of the observed chemo- and regioregioselectivity.

Recycling of **1** showed 95% retention of activity after **3** cycles, with the activity declining steadily over subsequent reuse, mainly attributable to mechanical losses (Figure S10, Supporting Information). Analysis of recycled catalyst by ^{13}C MAS NMR spectroscopy shows the presence of Cp* ligands (Figure S11, Supporting Information) and an essentially identical spectrum to freshly prepared **1**, indicating that the iridium fragment remained essentially unchanged.

Overall, the characterization data of **1** and **2** are consistent with coordination of [Cp*IrCl]+ to g-C$_3$N$_4$ via two adjacent N-donors (Figure 6). For **1**, an alternative binding mode exhibiting monodentate coordination giving [Cp*IrCl$_2$(g-C$_3$N$_4$-κ^1 N)] was excluded, based on the similarity of the spectroscopic data and zeta potentials of **1** and **2**. The distribution of iridium fragments is determined by the available binding sites that can accommodate [Cp*IrCl]+. Intercalation is excluded based on the PXRD data, which show an interplanar distance of 3.25 Å for **1** and **2**, which is essentially identical to that determined for g-C$_3$N$_4$. An estimated diameter of 6.5 Å for [Cp*IrCl]+, based on the X-ray single crystal structure of **3** limits coordination to exposed edge sites on the surface of the material because coincident g-C$_3$N$_4$ plane edges would be sterically too hindered. The iridium loading of 1.34 wt% compares to 7.34 wt% rhenium loading for [ReCl(CO)$_3$(g-C$_3$N$_4$-κ^2 N, N')],[7] where the estimated diameter of the ReCl(CO)$_3$ moiety is 5.5 Å, significantly smaller than [Cp*IrCl]+. The implication is that lower loading is associated with restricted access to additional potential binding sites indicating that steric non-covalent interactions control loading of the metal complex. The catalytic activity of **1** and **2** is limited to terminal alkenes, which is consistent with the congested steric environment, which likely limits the reaction rate, but nonetheless results in excellent chemo and regioselectivity for direct hydrogenation of terminal alkenes.

Conclusion

The maximum loading of g-C$_3$N$_4$ with metal complex fragments bound directly via κ^2 N, N' coordination is determined by the size of the metal fragment, suggesting that the number of available binding sites is defined by their steric environment. This is consistent with the complex microstructure of g-C$_3$N$_4$ arising from incomplete condensation and the formation of aggregates of low crystallinity. For [Cp*IrCl(g-C$_3$N$_4$ -κ^2 N, N')]Cl the restricted steric environment leads to selective catalysis for the hydrogenation of terminal alkenes. Characterization after catalysis also shows that the metal complex fragments are retained, and that the catalyst

has not undergone degradation or transformation to catalytically-active nanoparticles. Opportunities clearly exist to modify the microstructure of g-C$_3$N$_4$ to tailor the loading and steric environment of directly coordinated metal complex catalysts.

Experimental Section

Synthesis of Carbon Nitride (g-C$_3$N$_4$): was achieved using a previously reported method. Characterization by elemental analysis, powder X-ray diffraction (PXRD), scanning electron microscopy (SEM) and infra-red (IR), ^{13}C solid state magic angle spinning NMR (MASNMR), UV-vis and X-ray photoelectron (XPS) are consistent with those reported (see Supporting Information).[36] Urea (31 g, 0.52 mol) was placed in a ceramic crucible, covered with a lid and heated to 550 °C in air (ramp rate of 5 °C / min) for 180 min to give raw g-C$_3$N$_4$ (1.93 g) as a pale yellow powder. Raw g-C$_3$N$_4$ (500 mg) was then placed in a Schlenk tube under nitrogen before addition of ammonia in ethanol (2 mol dm^{-3}, 20 mL). The mixture was stirred for 3 hr before isolation by filtration. Base-treated g-C$_3$N$_4$ was then washed with ethanol (3 x 10 mL), water (3 x 10 mL), then ethanol (3 x 10 mL) and dried at 80 °C overnight to give g-C$_3$N$_4$ as a pale yellow powder. ^{13}C CP-MAS NMR (10 kHz, 125 MHz, 300 K, adamantane): δ= 164, 156 ppm; IR (ATR): ν = 3164, 1621, 1557, 1416, 1321, 1240, 1151, 806, 557 cm^{-1}; Anal. calcd (%) for C$_3$N$_4$: C, 39.14; H, 0; N, 60.86.; found C, 33.74; H, 1.75; N, 59.57. Formula: C$_3$N$_{4.54}$H$_{1.86}$

Synthesis of [Cp*IrCl(g-C$_3$N$_4$ −κ^2 N, N')]Cl (1): [IrCp*Cl$_2$]$_2$ (30 mg, 0.378 mmol) and g-C$_3$N$_4$ (200 mg) were refluxed in ethanol (10 mL) under nitrogen for 24 hrs. The mixture was filtered using a cannula, washed with ethanol (3 x 10 mL), and residual volatiles were removed under vacuum to give **1** as a yellow powder. Yield: 174 mg (75%). ICP-MS: Ir = 1.34; Cl = 0.37 wt%;

Synthesis of [Cp*IrCl(g-C$_3$N$_4$ −κ^2 N, N')][PF$_6$] (2): In dichloromethane (10 mL) under nitrogen [IrCp*Cl$_2$]$_2$ (58 mg, 0.07 mmol) and Ag[PF$_6$] (38 mg, 0.15 mmol) were stirred for 1 h to give a mixture of white AgCl precipitate and a yellow solution of [IrCp*Cl][PF$_6$]. The mixture was separated by cannula filtration and the filtrate added to g-C$_3$N$_4$ (200 mg) that had been placed under vacuum for 1 h at 100 °C before cooling to room temperature. The mixture was then refluxed under nitrogen for 24 h and separated by cannula filtration and washed with dichloromethane (2 x 10 mL) to give 2 as a finely yellow powder. Yield (based on g-C$_3$N$_4$): 170 mg (85%). ICP-MS: Ir = 1.33; Cl = 0.21 wt%; ion-chromatography F = 1.9 wt%;

Synthesis of [Cp*IrCl(DMNA−κ^2 N, N')][PF$_6$] (3): To [IrCp*Cl$_2$]$_2$ (117 mg, 0.15 mmol) dissolved in dichloromethane (5 mL) under nitrogen, was added a solution of DMNA (51 mg, 0.30 mmol) in dimethylformamide (1.8 mL) and the mixture was stirred at room temperature for 15 min. A solution of Ag(PF$_6$) (74 mg, 0.30 mmol) in methanol (2 mL) was then added and after stirring for 1.5 h, the mixture was filtered and the volatiles removed from the filtrate under reduced pressure to give a yellow solid which was recrystallizsed from acetonitrile/diethyl ether to give **3** as a yellow microcrystalline solid. Yield: 109 mg (54%). ^{1}H NMR (CDCl$_3$, 400 MHz, 297 K , TMS): δ= 8.29 (d, 9.6 Hz, 1H, CH), 7.25, (s, 1H, CH), 7.06 (d, 9.6 Hz, 1H, CH), 2.62 (s, 6H, CH3), 1.85 ppm (s, 15H, Cp*-CH3); ^{13}C CP-MAS NMR (10 kHz, 100 MHz, 297 K, adamantane): δ = 159.9, 157.0, 149.1, 134.8, 124.0, 114.9, 87.8 (Cp*-CCH$_3$), 24.8, 18.8, 9.9 ppm (Cp*-CCH$_3$); HRMS (ESI): m/z: calcd. for [^{12}C$_{20}$H$_{26}$^{35}Cl^{193}Ir^{14}N$_3$]+ 536.1447, found 536.1447; Anal. calcd (%) for C$_{20}$H$_{26}$ClF$_6$IrN$_3$P: C, 35.27, H, 3.85, N, 6.17. Found C, 34.95, H, 3.71, N, 6.04.

Crystallography: 1944187 (**3**) contains the supplementary crystallographic data for this paper. These data are provided free of charge by The Cambridge Crystallographic Data Centre.

Catalytic Hydrogenation: A glass vial (2 mL) was loaded successively with catalyst (2.0 μmol Ir, ca. 25 mg **1** and **2**, 1.4 mg **3**, and 0.7 mg

[IrCp*Cl₂]₂), substrate (0.2 mmol), hexane (1 mL) and a stirrer bar. The vial was then placed in a steel autoclave and charged with 10 bar hydrogen and stirred for 1 hr at room temperature. After reaction, a 0.2 mL aliquot was removed, diluted to 1 mL with hexane and analysed by GC. Calibration curves were obtained of all substrates and products in hexane.

Catalytic Hydrogenation with D₂: A vial of catalyst, solvent and substrate was placed in a steel autoclave and charged with 4 bar hydrogen. The pressure was then increased to 8 bar by addition of deuterium, and the reaction stirred for 3 hr at room temperature.

Recycling Studies: Recycling studies with **1** were performed by removing volatiles under reduced pressure and the residue used in a subsequent reaction.

[1] a) W.-J. Ong, L.-L. Tan, Y. H. Ng, S.-T. Yong, S.-P. Chai, *Chem. Rev.* **2016**, *116*, 7159-7329; b) Y. Wang, X. Wang, M. Antonietti, *Angew. Chem. Int. Ed.* **2012**, *51*, 68-89; c) Z. X. Zhou, Y. Y. Zhang, Y. F. Shen, S. Q. Liu, Y. J. Zhang, *Chem. Soc. Rev.* **2018**, *47*, 2298-2321; d) B. Zhu, L. Zhang, B. Cheng, J. Yu, *Appl. Catal B-Environ* **2018**, *224*, 983-999.

[2] Z. Chen, S. Mitchell, E. Vorobyeva, R. K. Leary, R. Hauert, T. Furnival, Q. M. Ramasse, J. M. Thomas, P. A. Midgley, D. Dontsova, M. Antonietti, S. Pogodin, N. López, J. Pérez-Ramírez, *Adv. Funct. Mater.* **2017**, *27*, 1605785.

[3] a) J. Kim, H.-E. Kim, H. Lee, **2018**, *11*, 104-113; b) G. Vile, D. Albani, M. Nachtegaal, Z. P. Chen, D. Dontsova, M. Antonietti, N. Lopez, J. Perez-Ramirez, *Angew. Chem.-Int. Edit.* **2015**, *54*, 11265-11269; c) P. Sharma, Y. Sasson, *Green Chem.* **2016**, *19*, 844-852; d) Q. Liu, J. Zhang, *Langmuir* **2013**, *29*, 3821-3828.

[4] a) X. Chen, J. Zhang, X. Fu, M. Antonietti, X. Wang, *J. Am. Chem. Soc.* **2009**, *131*, 11658-11659; b) J. Ma, Q. Yang, Y. Wen, W. Liu, *Appl. Catal B-Environ* **2017**, *201*, 232-240; c) J. Ma, N. Jia, C. Shen, W. Liu, Y. Wen, *J. Hazard. Mater.* **2019**, *378*, 120782.

[5] X. Wang, K. Maeda, A. Thomas, K. Takanabe, G. Xin, J. M. Carlsson, K. Domen, M. Antonietti, *Nat Mater* **2009**, *8*, 76-80.

[6] a) C. A. Caputo, M. A. Gross, V. W. Lau, C. Cavazza, B. V. Lotsch, E. Reisner, *Angew. Chem. Int. Ed.* **2014**, *53*, 11538-11542; b) R. Kuriki, K. Maeda, *Phys. Chem. Chem. Phys.* **2017**, *19*, 4938-4950.

[7] B. Coulson, M. Isaacs, L. Lari, R. E. Douthwaite, A. K. Duhme-Klair, *Chem. Commun.* **2019**, *55*, 7450-7453.

[8] a) S. Hohloch, L. Suntrup, B. Sarkar, *Organometallics* **2013**, *32*, 7376-7385; b) A. Ruff, C. Kirby, B. C. Chan, A. R. O'Connor, *Organometallics* **2016**, *35*, 327-335; c) C. Segarra, E. Mas-Marza, J. A. Mata, E. Peris, *Adv. Synth. Catal.* **2011**, *353*, 2078-2084; d) S. Thangavel, H. B. Friedrich, B. Omondi, *Mol. Catal.* **2017**, *429*, 27-42; e) D. Wang, D. Astruc, *Chem. Rev.* **2015**, *115*, 6621-6686; f) X. Wu, X. Li, A. Zanotti-Gerosa, A. Pettman, J. Liu, A. J. Mills, J. Xiao, *Chem. Eur. J.* **2008**, *14*, 2209-2222; g) J. H. Xie, S. F. Zhu, Q. L. Zhou, *Chem. Rev.* **2011**, *111*, 1713-1760.

[9] a) A. H. Ngo, M. J. Adams, L. H. Do, *Organometallics* **2014**, *33*, 6742-6745; b) Z. W. Xu, P. F. Yan, H. X. Li, K. R. Liu, X. M. Liu, S. Y. Jia, Z. C. Zhang, *ACS Catal.* **2016**, *6*, 3784-3788.

[10] a) N. Onishi, S. A. Xu, Y. Manaka, Y. Suna, W. H. Wang, J. T. Muckerman, E. Fujita, Y. Himeda, *Inorg. Chem.* **2015**, *54*, 5114-5123; b) Y. Suna, Y. Himeda, E. Fujita, J. T. Muckerman, M. Z. Ertem, *ChemSusChem* **2017**, *10*, 4535-4543; c) N. Onishi, R. Kanega, E. Fujita, Y. Himeda, *Adv. Synth. Catal.* **2019**, *361*, 289-296; d) M. Erlandsson, V. R. Landaeta, L. Gonsalvi, M. Peruzzini, A. D. Phillips, P. J. Dyson, G. Laurenczy, *Eur. J. Inorg. Chem.* **2008**, 620-627.

[11] A. Thomas, A. Fischer, F. Goettmann, M. Antonietti, J.-O. Müller, R. Schlögl, J. M. Carlsson, *J. Mater. Chem.* **2008**, *18*, 4893-4908.

[12] K. Park, G. H. Gunasekar, N. Prakash, K.-D. Jung, S. Yoon, *ChemSusChem* **2015**, *8*, 3410-3413.

[13] G. H. Gunasekar, S. Yoon, *J. Mater. Chem. A* **2019**, *7*, 14019-14026.

[14] G. Gunniya Hariyanandam, D. Hyun, P. Natarajan, K.-D. Jung, S. Yoon, *Catal. Today* **2016**, *265*, 52-55.

[15] Y. Hu, Y. Shim, J. Oh, S. Park, S. Park, Y. Ishii, *Chem. Mater.* **2017**, *29*, 5080-5089.

[16] P. Xia, B. Zhu, J. Yu, S. Cao, M. Jaroniec, *J. Mater. Chem. A* **2017**, *5*, 3230-3238.

[17] a) M. Majumdar, A. Sinha, T. Ghatak, S. K. Patra, N. Sadhukhan, S. M. W. Rahaman, J. K. Bera, *Chem. Eur. J.* **2010**, *16*, 2574-2585; b) S. Saha, M. Kaur, J. K. Bera, *Organometallics* **2015**, *34*, 3047-3054; c) S. Jin, D. Wang, *Acta Crystallogr. E* **2007**, *63*, M3036-U1601; d) S. Jin, D. Wang, Y. Sun, M. Guo, *Acta Crystallogr. E* **2007**, *63*, M3082-U2007; e) S. W. Jin, Y. Sun, *Acta Crystallogr. E* **2008**, *64*, M136-U1321; f) S. W. Jin, Q. J. Zhao, X. G. Qian, R. X. Chen, Y. F. Shi, *Acta Crystallogr. E* **2008**, *64*, M54-U561; g) M. Majumdar, S. M. W. Rahaman, A. Sinha, J. K. Bera, *Inorg. Chim. Acta* **2010**, *363*, 3078-3087.

[18] T. Suzuki, *Inorg. Chim. Acta* **2006**, *359*, 2431-2438.

[19] L. Dadci, H. Elias, U. Frey, A. Hoernig, U. Koelle, A. E. Merbach, H. Paulus, J. S. Schneider, *Inorg. Chem.* **1995**, *34*, 306-315.

[20] a) F. W. Monnard, E. S. Nogueira, T. Heinisch, T. Schirmer, T. R. Ward, *Chem. Sci.* **2013**, *4*, 3269-3274; b) F. Schwizer, V. Köhler, M. Dürrenberger, L. Knörr, T. R. Ward, *ACS Catal.* **2013**, *3*, 1752-1755; c) M. Hestericová, M. R. Correro, M. Lenz, P. F. X. Corvini, P. Shahgaldian, T. R. Ward, *Chem. Commun.* **2016**, *52*, 9462-9465; d) D. J. Raines, J. E. Clarke, E. V. Blagova, E. J. Dodson, K. S. Wilson, A. K. Duhme-Klair, *Nat. Catal.* **2018**, *1*, 680-688.

[21] P. Sudakar, G. H. Gunasekar, I. H. Baek, S. Yoon, *Green Chem.* **2016**, *18*, 6456-6461.

[22] a) G. H. Gunasekar, K. Park, V. Ganesan, K. Lee, N.-K. Kim, K.-D. Jung, S. Yoon, *Chem. Mater.* **2017**, *29*, 6740-6748; b) G. Gunniya Hariyanandam, D. Hyun, P. Natarajan, K.-D. Jung, S. Yoon, *Catal. Today* **2016**, *265*, 52-55.

[23] a) S.-L. Li, H. Yin, X. Kan, L.-Y. Gan, U. Schwingenschlogl, Y. Zhao, *Phys. Chem. Chem. Phys.* **2017**, *19*, 30069-30077; b) Y. Wang, J. Mao, X. G. Meng, L. Yu, D. H. Deng, X. H. Bao, *Chem. Rev.* **2019**, *119*, 1806-1854; c) Y. T. Gong, M. M. Li, H. R. Li, Y. Wang, *Green Chem.* **2015**, *17*, 715-736.

[24] a) Y. Li, Y. T. Gong, X. Xu, P. F. Zhang, H. R. Li, Y. Wang, *Catal. Commun.* **2012**, *28*, 9-12; b) D. S. Deng, Y. Yang, Y. T. Gong, Y. Li, X. Xu, Y. Wang, *Green Chem.* **2013**, *15*, 2525-2531; c) T. Yuan, H. F. Gong, K. Kailasam, Y. X. Zhao, A. Thomas, J. J. Zhu, *J. Catal.* **2015**, *326*, 38-42; d) Y. Wang, J. Yao, H. R. Li, D. S. Su, M. Antonietti, *J. Am. Chem. Soc.* **2011**, *133*, 2362-2365; e) Y. Li, X. Xu, P. F. Zhang, Y. T. Gong, H. R. Li, Y. Wang, *RSC Adv.* **2013**, *3*, 10973-10982; f) R. Arrigo, M. E. Schuster, S. Abate, G. Giorgianni, G. Centi, S. Perathoner, S. Wrabetz, V. Pfeifer, M. Antonietti, R. Schlogl, *ACS Catal.* **2016**, *6*, 6959-6966; g) Y. T. Gong, P. F. Zhang, X. Xu, Y. Li, H. R. Li, Y. Wang, *J. Catal.* **2013**, *297*, 272-280; h) H. Park, J. H. Lee, E. H. Kim, K. Y. Kim, Y. H. Choi, D. H. Youn, J. S. Lee, *Chem. Commun.* **2016**, *52*, 14302-14305; i) J. H. Lee, J. Ryu, J. Y. Kim, S. W. Nam, J. H. Han, T. H. Lim, S. Gautam, K. H. Chae, C. W. Yoon, *J. Mater. Chem. A* **2014**, *2*, 9490-9495.

[25] X. F. Chen, L. G. Zhang, B. Zhang, X. C. Guo, X. D. Mu, *Sci Rep* **2016**, *6*, 13.

[26] D. Albani, M. Shahrokhi, Z. P. Chen, S. Mitchell, R. Hauert, N. Lopez, J. Perez-Ramirez, *Nat. Commun.* **2018**, *9*, 11.

[27] Z. K. Zhao, H. L. Yang, *J. Mol. Catal. A-Chem.* **2015**, *398*, 268-274.

[28] X. H. Huang, Y. J. Xia, Y. J. Cao, X. S. Zheng, H. B. Pan, J. F. Zhu, C. Ma, H. W. Wang, J. J. Li, R. You, S. Q. Wei, W. X. Huang, J. L. Lu, *Nano Res.* **2017**, *10*, 1302-1312.

[29] S. B. Tian, W. B. Gong, W. X. Chen, N. Lin, Y. Q. Zhu, Q. C. Feng, Q. Xu, Q. Fu, C. Chen, J. Luo, W. S. Yan, H. J. Zhao, D. S. Wang, Y. D. Li, *ACS Catal.* **2019**, *9*, 5223-5230.

[30] S. B. Tian, Z. Y. Wang, W. B. Gong, W. X. Chen, Q. C. Feng, Q. Wu, C. Chen, C. Chen, Q. Peng, L. Gu, H. J. Zhao, P. Hu, D. S. Wang, Y. D. Li, *J. Am. Chem. Soc.* **2018**, *140*, 11161-11164.

[31] R. Ciriminna, M. Lomeli-Rodriguez, P. D. Cara, J. A. Lopez-Sanchez, M. Pagliaro, *Chem. Commun.* **2014**, *50*, 15288-15296.

[32] G. Rubulotta, K. L. Luska, C. A. Urbina-Blanco, T. Eifert, R. Palkovits, E. A. Quadrelli, C. Thieuleux, W. Leitner, *ACS Sustain. Chem. Eng.* **2017**, *5*, 3762-3767.

[33] J. Morere, E. Sanchez-Miguel, M. J. Tenorio, C. Pando, A. Cabanas, *J. Supercrit. Fluids* **2017**, *120*, 7-17.

[34] S. Agarwal, J. N. Ganguli, *J. Mol. Catal. A-Chem.* **2013**, *372*, 44-50.

[35] E. Bogel-Lukasik, S. Santos, R. Bogel-Lukasik, M. N. da Ponte, *J. Supercrit. Fluids* **2010**, *54*, 210-217.

[36] Y. Zhang, J. Liu, G. Wu, W. Chen, *Nanoscale* **2012**, *4*, 5300-5303.

Entry for the Table of Contents
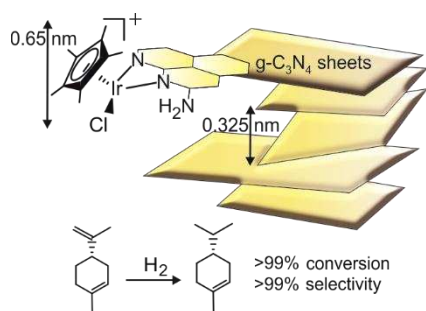
Selective catalytic hydrogenation of terminal alkenes is observed when [Cp*IrCl]$^+$ is supported on g-C$_3$N$_4$. Direct coordination of [Cp*IrCl]$^+$ to g-C$_3$N$_4$ occurs via κ^2 N, N' binding and is limited to exposed edge sites. The restricted steric environment at the Ir atom results in slow but highly selective catalysis.